

# LAT Aerospace

Team 99

# Executive Summary

Our task is to design a high-lift wing and propulsion mechanism configuration for an STOL aircraft. For proceeding towards this problem statement, we begin by mathematically modeling the core components of an aircraft - namely the Thrust Plant (or the Propulsion system) and the Wing. As we refine our mathematical concept, we continuously and iteratively verify our results using Computational Fluid Dynamics Techniques.

Our preliminary research lead us to a hypothesis, that for an STOL aircraft of the scale required by LAT Aerospace, a Distributed Electric Propulsion (DEP) system, composed of Propellers driven by Brushless Electric Motors is the most optimal thrust device. To utilize this mechanism most efficiently, this mechanism to be coupled with optimally designed wings and control surfaces.

Standard wings cannot provide enough lift to take off at such low speeds as desired, thus exotic mechanisms are integrated to achieve desired performance indices. Blown Flaps, Upper Surface Blown Wings, etc. are some extensively researched topics that can enhance the lift capability of aircraft. Our research finds Blown Flaps to be optimal, because of the mechanical simplicity, and higher efficiencies than other mechanisms.

In our research we focused on accurately refining our mathematical formulation for the above devices, and an attempt to parameterize the equations, in order to allow us to use constraint optimization techniques to get optimal configurations of the aforementioned components.

In this paper, we were able to mathematically model the propellers and the blown wings to a great level of accuracy, with sufficient parameterization which we can run over by the use of iterative optimization techniques. This allowed us to obtain the targeted values of our coefficients of lift, and the lift-by-drag ratios.

For reaching the solution, we used tools like ANSYS (Student) for Computational Fluid Dynamics, XFOIL for getting airfoil characteristics, and Python and its libraries (e.g. SciPy, NumPy, etc.) for mathematically modeling the components and for designing the constraint optimization problems. Initially we also used open source tools like OpenVSP and AVL, but on recommendation by the company officials we diverted our efforts towards the other core tools.

# Contents

<b>1 A Review of Different Configurations of Wings</b>	<b>1</b>
1.1 Introduction . . . . .	1
1.2 The Cluster Channel Wing . . . . .	1
1.3 Prandtl-D (Bell Spanload) . . . . .	2
1.4 Joint Wings . . . . .	3
1.5 Selected Architecture: DEP & Blown Flaps . . . . .	4
1.6 Aerodynamic Superiority . . . . .	4
1.7 Why DEP Wins . . . . .	5
1.8 Conclusion . . . . .	5
<b>2 Thrust Plant</b>	<b>6</b>
2.1 Introduction . . . . .	6
2.2 Propeller . . . . .	7
2.2.1 Mathematical Model . . . . .	7
2.2.1.1 Momentum Theory . . . . .	8
2.2.1.2 Blade Element Momentum theory . . . . .	10
2.2.2 Validation From Experimental Results . . . . .	12
2.2.2.1 Experiment setup . . . . .	12
2.2.2.2 Results . . . . .	12
2.3 EDF . . . . .	14
<b>3 Wing</b>	<b>15</b>
3.1 Introduction . . . . .	15
3.2 Wing Without Flaps . . . . .	15
3.2.1 Overview . . . . .	15
3.2.2 Mathematical Model . . . . .	15
3.3 Wing With Flaps . . . . .	18
3.3.1 Overview . . . . .	18
3.3.2 Mathematical Model . . . . .	18
3.4 Blown Wing With Flaps . . . . .	19
3.4.1 Overview . . . . .	19
3.4.2 Mathematical Model . . . . .	19
3.5 Finite Blown Wing with Flaps . . . . .	23
3.5.1 Numerical Model . . . . .	23

<b>4 Computational Fluid Dynamics</b>	<b>25</b>
4.0.1 Validation of Propulsion using Computational Fluid Dynamics . . . . .	25
4.0.1.1 Geometry Construction and Meshing . . . . .	25
4.0.1.2 Setup . . . . .	25
4.0.1.3 Results and Discussion . . . . .	26
4.0.2 Validation of Wing Design using Computational Fluid Dynamics . . . . .	27
4.0.2.1 Geometry Construction and Meshing . . . . .	27
4.0.2.2 Setup . . . . .	28
4.0.2.3 Results and Discussion . . . . .	28
4.0.3 Adding Flaps . . . . .	29
4.0.3.1 Results and Discussion . . . . .	30
4.0.4 Validation of Blowing Characteristics using Computational Fluid Dynamics . . . . .	30
4.0.4.1 Geometry Construction and Meshing . . . . .	31
4.0.4.2 Setup . . . . .	31
4.0.4.3 Results and Discussion . . . . .	32
<b>5 Final Results</b>	<b>33</b>
5.0.1 Introduction . . . . .	33
5.0.2 Propeller Geometry . . . . .	33
5.0.3 Airfoil Geometry . . . . .	33
5.0.4 Take Off Configuration . . . . .	33
5.0.5 Cruise Configuration . . . . .	34
<b>6 Structural Analysis</b>	<b>37</b>
<b>7 End Comments</b>	<b>40</b>
7.1 Additional Features . . . . .	40
7.1.1 Inboard-Up Rotation Mechanism . . . . .	40
7.1.2 Tilting Down of the Propeller . . . . .	40
7.1.3 Counter Rotating Blades or Wing twist . . . . .	40
<b>Bibliography</b>	<b>41</b>

# Chapter 1

## A Review of Different Configurations of Wings

### 1.1 Introduction

In this section we will be looking into a few different configurations of wings and propellers and how we ended up with choosing the method of Distributed Electric Propulsion (DEP) for our aircraft.

### 1.2 The Cluster Channel Wing

The Channel Wing, developed by Willard Custer in the 1940s, features a semi-circular channel formed into the wing structure, with a propeller placed at the trailing edge. Unlike a ducted fan, the channel is an open airfoil section (typically a NACA 4418 or similar reflexed airfoil) curled into a semi-circle.

- **Suction Mechanism:** The propeller acts as an aspirator, drawing air through the channel at high velocity  $V_{\text{local}}$ .
- **Pressure Differential:** According to  $P + \frac{1}{2}\rho V^2 = \text{constant}$ , the high velocity inside the channel creates a deep low-pressure zone on the upper wing surface.
- **Result:** Lift is generated by engine RPM rather than aircraft airspeed  $V_\infty$ . Custer claimed lift coefficients  $C_L > 5.0$ , whereas conventional wings stall near  $C_L \approx 1.5$ .

However, there are a few drawbacks to this method such as-

- **Catastrophic Asymmetry:** In a twin-engine configuration, an engine failure results in the immediate loss of lift on one side (not just thrust).
- **Parasitic Drag:** The large wetted surface area significantly increases form and skin friction drag during cruise.
- **Structural Rigidity:** Maintaining the small prop–channel gap requires a heavy, stiff structure. Wing flex may cause a catastrophic prop-strike.



Figure 1.1: The propeller draws air through the channel, creating lift even at zero airspeed.

### 1.3 Prandtl-D (Bell Spanload)

Based on the 1933 work of Ludwig Prandtl and refined by NASA's Albion Bowers, the Prandtl-D (Preliminary Research Aerodynamic Design to Lower Drag) uses a Bell-shaped span load instead of the traditional elliptical loading.

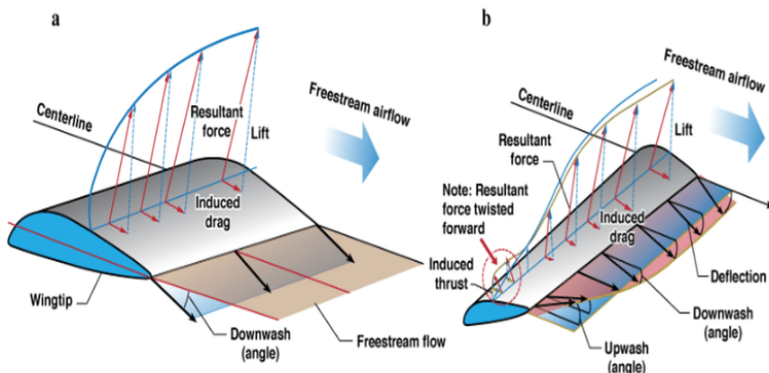


Figure 1.2: The Bell spanload reduces wing root bending moment, allowing longer wings.

- **Induced Drag Reduction:** For fixed structural weight, Bell loading reduces induced drag by  $\sim 11\%$  due to increased allowable span.
- **Proverse Yaw:** Wingtips experience local upwash, tilting the lift vector forward and producing yaw-stabilizing thrust.
- **Tailless Efficiency:** Enables removal of vertical tail surfaces.

Few drawbacks of this model are:

- **Control Authority:** Yaw control via wing twist is sluggish, problematic for crosswind operations.
- **Manufacturing Complexity:** The nonlinear geometric twist is expensive and difficult to fabricate.
- **Payload Integration:** Poor internal volume efficiency for cargo or multipassenger missions.

## 1.4 Joint Wings

This configuration consists of a swept-back front wing joined at the tips to a swept-forward rear wing, forming a diamond or box shape in the planform.

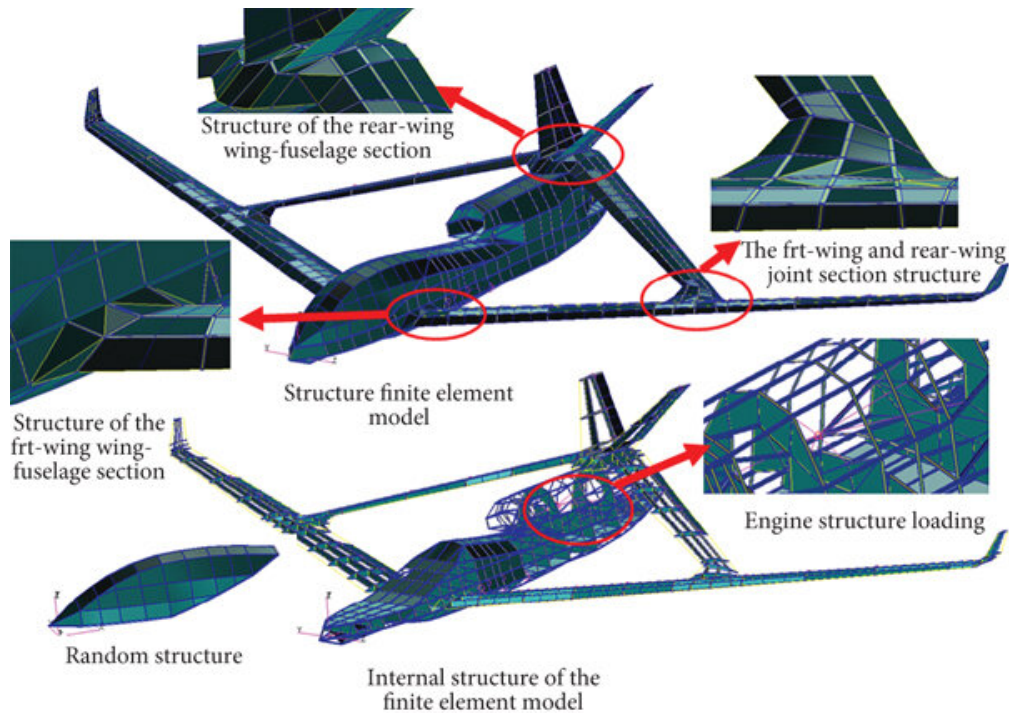


Figure 1.3: The joined wing creates a rigid box structure.

Given below are some of the properties of the Joint Wing

- **Structural Efficiency:** The rear wing acts as a strut, bracing the front wing. This allows for extremely high Aspect Ratios ( $AR > 20$ ) without the weight penalty of a cantilever wing.
- **Vortex Suppression:** The closed wing system physically inhibits the formation of high-energy wingtip vortices, increasing the effective span efficiency ( $e$ ).

However, due to the presence of a few drawbacks, we have had to reject this design

- **Interference Drag:** The junction points where the wings meet create complex aerodynamic interference. The boundary layers of both wings merge, leading to premature flow separation and high drag.
- **Aeroelastic Instability:** The over-constrained structure is prone to complex flutter modes. Thermal expansion differences between the wings can cause buckling, requiring heavy joint reinforcements.

## 1.5 Selected Architecture: DEP & Blown Flaps

The selected design utilizes **Distributed Electric Propulsion (DEP)** combined with large-span **Blown Flaps**. This system employs multiple electric motors along the leading edge to actively accelerate air over the wing<sup>[1]</sup>.



Figure 1.4: DEP increases dynamic pressure over the wing, independent of airspeed.

## 1.6 Aerodynamic Superiority

This configuration was selected as it combines the high-lift benefits of the Channel Wing with the controllability of conventional aircraft.

- **Boundary Layer Control:** The high-velocity prop-wash energizes the boundary layer, preventing flow separation at extreme angles of attack (up to 40°).
- **Dynamic Pressure Rise:** The propellers increase the dynamic pressure ( $q$ ) over the wing. Since Lift  $L = C_L \cdot q \cdot S$ , increasing  $q$  directly increases lift without needing to increase wing area ( $S$ ).

- **Super-Circulation:** The accelerated flow increases the circulation ( $\Gamma$ ) around the wing. Per the Kutta-Joukowski theorem ( $L = \rho V \Gamma$ ), this drastically increases lift capacity ( $C_{L_{max}} > 4.5$ ).

## 1.7 Why DEP Wins

- **Decoupled Lift:** Like the Channel Wing, lift is generated by power setting, not just airspeed, enabling STOL.
- **Safety:** Unlike the Channel Wing, the distributed nature of DEP means a single motor failure results in negligible lift asymmetry.
- **Control:** The prop-wash flows over the control surfaces (flaps/ailerons), ensuring high control authority even at near-zero flight speeds.

## 1.8 Conclusion

While passive geometric concepts like the Prandtl-D and Joined Wing offer theoretical drag reductions, they lack the low-speed control authority and manufacturing simplicity required. The Custer Channel Wing offers high lift but introduces unacceptable safety risks.

Therefore, the **DEP with Blown Flaps** architecture is the optimal solution. It provides active high-lift generation, robust control authority, and a fail-safe redundancy that passive configurations cannot match.

# Chapter 2

## Thrust Plant

### 2.1 Introduction

One of the first components of an aircraft we need to start working on is the Thrust Plant, which may also be called the Propulsion System. These systems provide the thrust to move the aircraft along the runway to build up speed, which is leveraged by the wings to provide the necessary lift for the aircraft to take off and stay in the air.

Thrust plants can broadly be classified into two categories, Non-Air Breathing Systems (like Rocket Engines, Ionic Propulsion, etc.) or Air Breathing Systems. The Air Breathing Systems in themselves can be classified into families based on what kind of technology runs them, like Gas-Turbine / Jet Engines (Turbofan, Turbojet, Turboprop, Ramjet, Scramjet, etc.) or Propulsive Disk Systems (Rotor-based, Propeller, Ducted Fan, etc.).

Thrust plants like Rocket Engines are not designed for atmospheric cruise flight and are highly inefficient for short-range transport as is desired. Others like Ionic Propulsion provide an extremely low Thrust-to-Weight ratios, which make them impractical for an aircraft. Within Air Breathing systems, Engines based on Gas-Turbines or Jet Engines are unsuitable for urban operations due to their extremely low efficiency in low-speed low-altitude conditions which we are targeting. Moreover, their high exhaust velocities result in excessive noise, heat and downwash, making them unfavorable for flight around residential and other urban regions.

This leaves the Propulsive Disk Systems, which generate thrust by imparting momentum to a large mass of air. These systems - comprising of Rotors, Propellers, and Electric Ducted Fans (EDFs) - are more efficient at low-speed flights. Other capabilities like electric drive integration make them ideal candidates for Distributed Electric Propulsion (DEP) architectures which are commonly used in other STOL aircrafts targeting a similar audience, like the ones made by Electra<sup>[2]</sup>.

In this Chapter we have covered Propellers and EDFs, and done a comparative study over why one must perform better than the other in our desired application. Rotor-based configurations were excluded from this analysis, as their design characteristics are more similar to vertical or hover-capable systems instead of fixed-wing aircrafts.

## 2.2 Propeller

The propulsion system is crucial to obtain very high and efficient lift. Three major types of propulsion systems were suggested to work upon that are Open Propellers, EDFs, and Rotors. Our work is majorly focused toward propellers as they are most suitable for the STOL configuration which we will justify through a qualitative analysis ahead.

To predict the performance of any propeller mathematically is difficult considering the airflow complexity that exists in a flight during take-off or Landing so we consider the propeller to be stationary and fixed in space. The major factors that affect the thrust it generates are: The blade geometry, Advance ratio and Airfoil used in the blade. The governing theorems and equations to solve all these factors are given by Navier Stokes Equations which are non-linear PDEs and difficult to solve. They can be simplified by various assumptions like inviscid, incompressible and steady flow but still they remain difficult to solve in 3 dimensions so we need to look into other theories to derive a mathematical model that can accurately predict a Propeller's performance. For this purpose we have considered Blade Element Momentum Theory which comprises of BET – Blade Element Theory and Momentum Theory that are used together.

The BET considers each blade section as a 2D airfoil to produce aerodynamic forces and by integrating these sectional loads over the length of the blade and averaging the result over a rotor revolution, we obtain the total thrust and torque of the propeller.

Momentum theory on the other hand deals with the propeller as a thin disk with some velocity and pressure distribution on its faces and at infinity. It basically comprises of conservation laws and deals with the work done on the fluid by the propeller.

Combining these theories we can make a mathematical model that includes all the factors which are not considered in any one of them.

### 2.2.1 Mathematical Model

The methods are derived from Winarto's<sup>[3]</sup> works. Let us assume a propeller of an aircraft which is cruising at some altitude in forward flight, it would feel a relative wind velocity axially, say at  $V \text{ m/s}$ , that is just the forward speed of the aircraft and the propeller is rotating at an angular speed, say,  $\Omega \text{ rad/s}$ . Then the relative velocity of the blade tip with respect to the wind will be

$$V_R = \sqrt{V^2 + (\Omega r)^2}$$

This is based on the assumption that the airfoil of blade has no effect on the wind velocity, which is not correct. As like any other airfoil, this will also generate some lift and drag force on the blade element which will affect the relative wind velocity. We account for this as axial and azimuthal induction factors say  $a$  and  $b$ , respectively, such that

$$V_R = \sqrt{(1+a)^2 V^2 + (1-b)^2 (\Omega r)^2}$$

This implies that the induced axial velocity produced by the blade element is  $aV$  and the azimuthal velocity is  $-b\Omega r$ . The angle made by the resultant velocity with propeller plane is

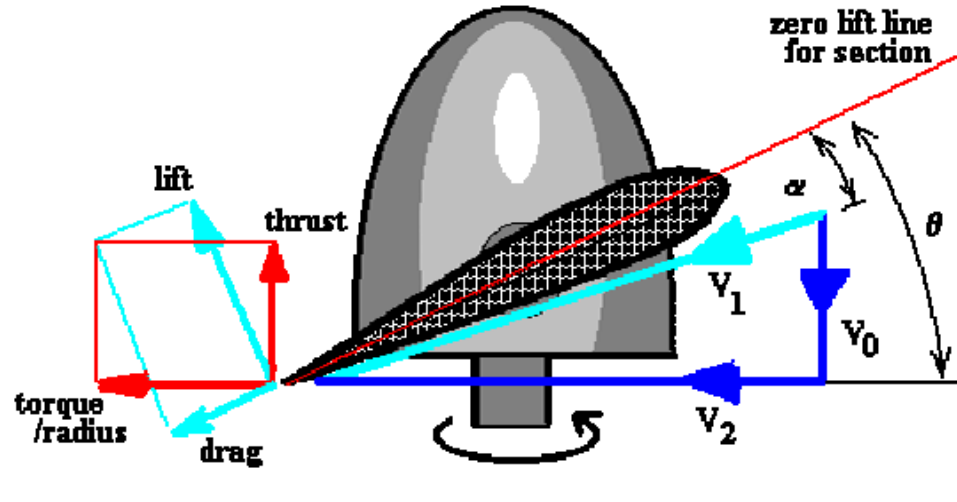
**Resultant Force Vectors****Flow Vectors**

Fig.2 Definition of flow and force directions on a blade element (from ref.1)

called the inflow angle  $\phi$ , such that

$$\tan \phi = \frac{(1+a)V}{(1-b)\Omega r}$$

$$\sin \phi = \frac{(1+a)V}{V_R}$$

$$\cos \phi = \frac{(1-b)\Omega r}{V_R}$$

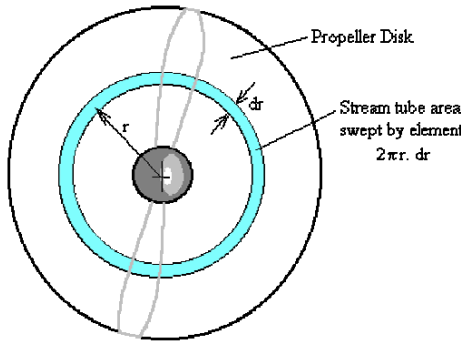
Thus, if we know the inflow angle we can easily find the induction factors and finally the resultant velocity at any blade element. We calculate these factors at a blade element which we assume to be independent of other blade elements and the lift generated by this element will only depend on the relative velocity of the wind that strikes it.

### 2.2.1.1 Momentum Theory

The aim of momentum theory is to find the radial distribution of the inflow angle. As stated, propeller geometry is not important for this. We assume a static disk and define the pressure and air velocities above and below the disk area to derive thrust and torque equations. Assume the pressure just above the disk is  $p_1$  and just below the disk  $p_2$  with the total area of disk  $A$ . Thus the thrust  $T$  experienced by the disk will be given by

$$T = A(p_2 - p_1) \quad (2.1)$$

According to law of conservation of momentum the thrust imparted by the air on the disk should be equal to the thrust imparted by the disk to the air which could be calculated with



air velocities near and far below the disk

$$T = \dot{m}(V_s - V) \quad (2.2)$$

here  $\dot{m}$  is the mass transfer rate and  $V_s$  is the velocity far downstream of disk.

$$\dot{m} = \rho V_0 A \quad (2.3)$$

$$p_2 - p_1 = \rho V_0 (V_s - V) \quad (2.4)$$

Since the flow is considered streamline we can apply Bernoulli equation, for the upward region of the disk

$$p_0 + \frac{1}{2}\rho V^2 = p_1 + \frac{1}{2}\rho V_0^2 \quad (2.5)$$

and for the downward region

$$p_2 + \frac{1}{2}\rho V_0^2 = p_0 + \frac{1}{2}\rho V_s^2 \quad (2.6)$$

now combining the two equations

$$p_2 - p_1 = \frac{1}{2}\rho(V_s^2 - V^2) \quad (2.7)$$

With previously defined velocity relations

$$V_0 = \frac{1}{2}(V_s + V) \quad (2.8)$$

$$V_0 = V(1 + a) \quad (2.9)$$

Now We divide the disk in small annuli and calculate the thrust produced by each one as

$$\Delta T = \rho V_0 2\pi r \Delta r (V_s - V) \quad (2.10)$$

$$\frac{dT}{dr} = 4\pi \rho r V^2 a (1 + a) \quad (2.11)$$

We can obtain the torque on the elemental disk as

$$dQ = \rho V_0 \cdot 2\pi r dr \cdot 2b\Omega r \quad (2.12)$$

$$\frac{dQ}{dr} = 4\pi\rho r^3 \Omega V_0 b \quad (2.13)$$

We can see that induced factors cannot be calculated by momentum theory alone but if determined, thrust and power can be easily calculated using momentum theory.

### 2.2.1.2 Blade Element Momentum theory

As the blade rotates with an angular speed of  $\Omega$ , the blade element is subjected to elemental lift and drag forces of  $dL$  and  $dD$  respectively. The values of those forces are given by

$$\Delta L = \frac{1}{2}\rho V_R^2 C_l c \Delta r \quad (2.14)$$

$$\Delta D = \frac{1}{2}\rho V_R^2 C_d c \Delta r \quad (2.15)$$

And the resultant force on the element is given by

$$dF_R = \sqrt{dL^2 + dD^2} = dL\sqrt{1 + \tan^2 \gamma} = dL \sec \gamma \quad (2.16)$$

where  $\gamma = \arctan(c_d/c_l)$ .

The resultant force can be resolved into 2 components, with one component being in the axial direction and the other in the azimuthal direction. The axial component of the force is the same as the elemental thrust force due to a single blade, and if the propeller has  $B$  blades then the elemental thrust of the propeller is

$$dT = dL \cos \phi - dD \sin \phi = \frac{1}{2}\rho V_R^2 B c dr (C_l \cos \phi - C_d \sin \phi) \quad (2.17)$$

$$dT = \frac{1}{2}\rho V_R^2 B c C_l dr (\cos \phi - \tan \gamma \sin \phi) \quad (2.18)$$

The azimuthal component of the elemental resultant force when multiplied by the radial distance  $r$ , is the elemental torque of the propeller.

$$\frac{dQ}{dr} = \frac{1}{2}B c \rho V_R^2 C_l r \sec \gamma \sin(\phi + \gamma) \quad (2.19)$$

Now that we have thrust and torque equation by two different methods and we can compare the two equations and solve for the inflow angle  $\phi$

The thrust equation can be written as

$$aV = \frac{1}{4}\sigma C_l \sec \gamma \csc \phi \cos(\phi + \gamma) V_R \quad (2.20)$$

Similarly, the equation for torque gives the following result

$$b\Omega r = \frac{1}{4}\sigma C_l \sec \gamma \csc \phi \sin(\phi + \gamma) V_R \quad (2.21)$$

We can write the equation for axial velocity as

$$V_R \sin \phi = V + \frac{1}{4}\sigma C_l \sec \gamma \csc \phi \cos(\phi + \gamma) V_R \quad (2.22)$$

on further simplifying it we can write it as a function of inflow angle

$$F(\phi) = \frac{V}{V_R} = \sin \phi - \frac{1}{4}\sigma C_l \sec \gamma \csc \phi \cos(\phi + \gamma) \quad (2.23)$$

$$V_R \cos \phi = \Omega r - \frac{1}{4}\sigma C_l \sec \gamma \csc \phi \sin(\phi + \gamma) V_R \quad (2.24)$$

$$G(\phi) = \frac{\Omega r}{V_R} = \cos \phi + \frac{1}{4}\sigma C_l \sec \gamma \csc \phi \sin(\phi + \gamma) \quad (2.25)$$

$$g(\phi) = (\Omega r \sin \phi - V \cos \phi) \sin \phi - \frac{1}{4}\sigma C_l \sec \gamma (\Omega r \cos(\phi + \gamma) + V \sin(\phi + \gamma)) \quad (2.26)$$

The equation is a transcendental equation in  $g(\phi)$  that can be solved for the required value of  $\phi$ . This equation must be solved numerically as an iterative method. Out of the several iterative methods we are using the Regula Falsi<sup>[4]</sup> method to determine inflow angle at each blade element.

After we get the inflow angle, we can easily calculate the thrust and torque as

$$\frac{dT}{dr} = \frac{1}{2} B c \rho V_R^2(\phi) [C_{l,\alpha} \alpha \cos \phi - C_d(\alpha) \sin \phi] \quad (2.27)$$

$$\frac{dQ}{dr} = \frac{1}{2} B c \rho V_R^2(\phi) [C_{l,\alpha} \alpha \sin \phi + C_d(\alpha) \cos \phi] r \quad (2.28)$$

Once we have the elemental thrust and torque we just need to integrate it over the span to obtain total thrust and torque experienced by the propeller

$$T = \Delta R \left[ \frac{1}{2} \left( \frac{dT}{dr} \right)_1 + \sum_{n=2}^N \left( \frac{dT}{dr} \right)_n \right] \quad (2.29)$$

$$Q = \Delta R \left[ \frac{1}{2} \left( \frac{dQ}{dr} \right)_1 + \sum_{n=2}^N \left( \frac{dQ}{dr} \right)_n \right] \quad (2.30)$$

Further the empirical corrections like Prandtl's tip loss factor and Glauert correction can be introduced to account for tip losses and critical axial induction factor. For the Blade Geometry we can optimize the power for certain thrust by keeping a linear twist along the blade according to Leishman<sup>[5]</sup>.

## 2.2.2 Validation From Experimental Results

The code thus produced from the mathematical model is validated using Experimental data from NACA wind tunnel testing [6] and results are pretty satisfactory. Below is the detailed description of the propeller modelling and experiment setup.

### 2.2.2.1 Experiment setup

The experiment was performed to compare efficiencies of two different blade elements namely NACA 16-series and Clark Y. It was conducted in 20 foot wind tunnel with two identical propellers having diameter of 10 foot.

The Propeller geometry and blade parameters are given below :

Table 2.1: Blade Geometry Definition: NACA TR 594 (Nose 6-Propeller C)

<b>Radius (m)</b>	<b>Chord (m)</b>	<b>Pitch (°)</b>	<b>Airfoil Section</b>
0.525	0.1800	17	Clark Y
0.675	0.2250	17	Clark Y
0.825	0.2250	17	Clark Y
0.975	0.2100	17	Clark Y
1.125	0.1875	17	Clark Y
1.275	0.1425	17	Clark Y
1.425	0.1200	17	Clark Y

### Global Parameters

Diameter	3.054 m
Number of Blades	3
Hub Radius	0.375 m

### 2.2.2.2 Results

These parameters are put in our mathematical model and graphs of efficiency, thrust coefficient and drag coefficient are plotted with respect to advance ratio to compare with the actual data. Note that the pitch is corrected by 2 degrees as stated in [7] to account for different conventions used today and as presented in [8]. Below are the graphs obtained with comparison. As we can see the efficiency was overestimated by the solver while power coefficient was underestimated but coefficient of thrust was almost identical. This is primarily because of the assumption that flow on any element does not affect the flow on nearby element. From the graphs, we can conclude that our code is more accurate for high advance ratio operations.

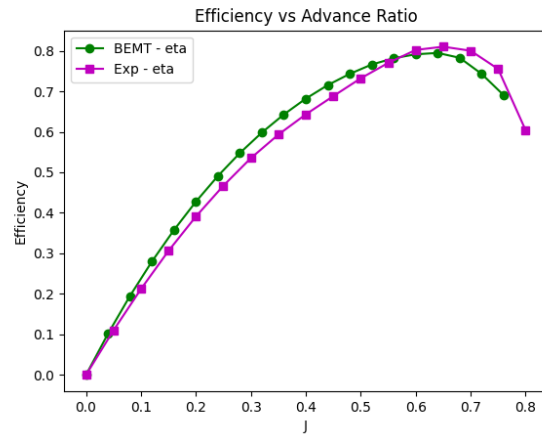


Figure 2.1: Enter Caption

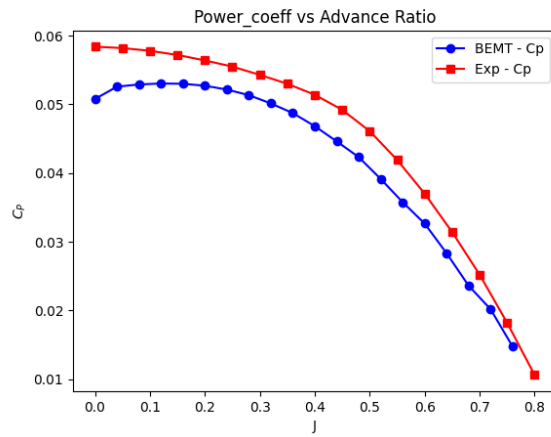


Figure 2.2: Enter Caption

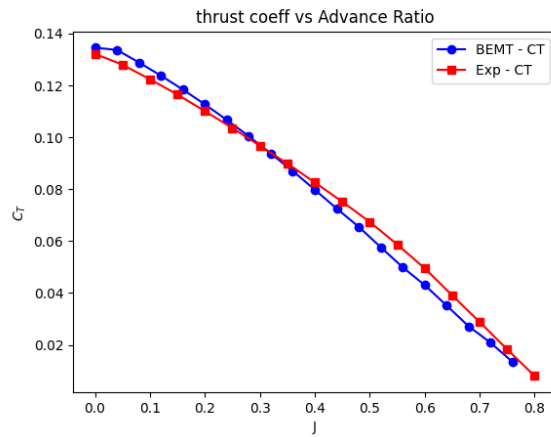


Figure 2.3: Enter Caption

## 2.3 EDF

Electric Ducted Fans are common Thrust Plants used in various kinds of aircrafts, but in our application, they have limited efficacy. From a technical point of view, the wetted area and geometric interferences of the duct add a lot of drag to the aircraft. They need to be designed specifically for the cruise conditions for improved system efficiency, that too at a higher airspeed, but only with reduced low-speed performance. This also acts as an additional component to be manufactured, with tight tolerances between the blade tip and internal surface, adding manufacturing and maintenance costs. EDFs also have a high disk loading, added weight and mechanical complexity. Internal flow in EDFs may be harder to inspect and repair.

EDFs also have certain advantages over a propeller, including a higher thrust production, reduced noise and added safety. If cruise speed is relatively high (not our case!), EDFs start to be competitive as flight speed climbs into higher ranges where the duct can reduce tip losses and the fan operates closer to its design point.

We analyzed several studies on EDFs which present both computational as well as experimental comparisons of EDFs with open propellers and the key findings were somewhat common in all of them that EDFs produce a better efficiency over open propellers but their main drawback is additional drag of duct and its design complexity which it certainly unsuitable for STOLs. But they can be used if installed as small distributed propulsors.

Below are the results of a study done by NASA<sup>[9]</sup>. They have setup a wind tunnel and tested the performances of a propeller with and without a duct. The results clearly demonstrate the superiority of propellers over EDFs.

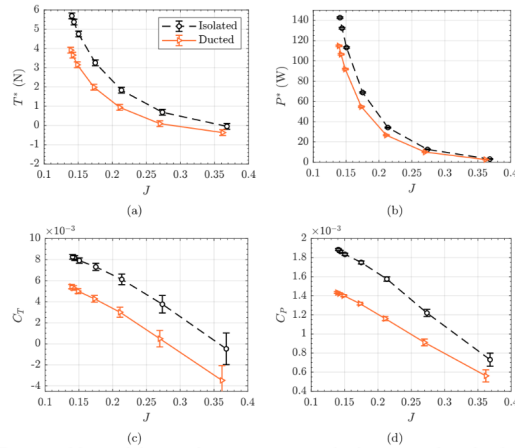


Figure 18. Measured thrust and power variations with advance ratio for isolated and ducted propeller configurations in simulated low-sped axial forward flight conditions.

Figure 2.4: Enter Caption

Thus for our Distributed Electric Propulsion (DEP) STOL, the winner in general is propellers - ideally many low-disk-loading, slow-turning propellers that blow the wing and flaps. EDFs may work, but they are generally worse for the low-speed high-static-thrust regime STOL needs.

# **Chapter 3**

## **Wing**

### **3.1 Introduction**

The Wing can undoubtedly be considered as one of the most important components for an STOL aircraft. Without an optimally designed wing, it is impossible to achieve high performance indices with any amount of thrust. Particularly in a STOL aircraft, a very high Coefficient of Lift  $C_L$  is required for the takeoff scenario, since our desire of shorter runway lengths leads to a lesser takeoff velocity for the aircraft.

In this Chapter, we have covered 3 basic scenarios of wings, which improve the coefficient of lift incrementally. We start with a simple infinite wing with a high lift airfoil like the NACA-4412. The high coefficients of lift desired for an STOL cannot be obtained by just using an optimal airfoil. For achieving higher lift, we will also be introducing flaps - which are the most common way of enhancing the lift. Further enhancements can be done by using the jet induced by our propulsion system and blowing it onto the wing and flap surface.

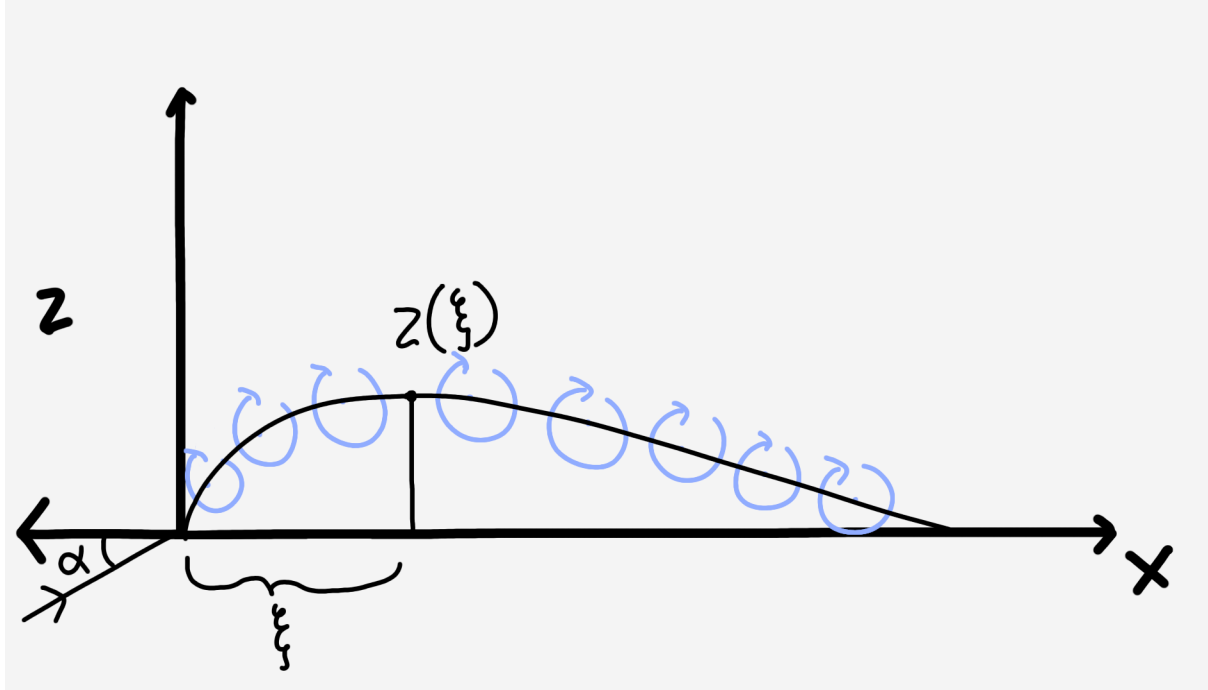
### **3.2 Wing Without Flaps**

#### **3.2.1 Overview**

In this section, our aim is to solve the coefficient of lift for a cambered airfoil. We do this through the implementation of the thin airfoil theory and the vortex sheet method. We use these methods because it allows us to solve and hence compare the change in the coefficient of lift in the case of a blown flap later.

#### **3.2.2 Mathematical Model**

In the vortex sheet method, we consider the airfoil to be made up of a series of vortices that form along the camber of the airfoil. This assumption allows us to calculate the circulation over the airfoil, which further allows us to calculate the lift and the coefficient of lift of the airfoil.<sup>[10]</sup>



Before starting our analysis, we are going to take certain assumptions so that we can arrive at a fairly accurate result with lesser complexity. We will assume that the airfoil to be thin and that we would operate at a small angle of attack  $\alpha$ . We will also consider the wingspan to be infinite as we are mainly focusing on the 2D analysis of the airfoil.

Now, we take the flow of air normal to the airfoil to be 0. Mathematically, this looks like

$$V_{\infty,n} + \omega'(s) = 0 \quad (3.1)$$

Where  $V_{\infty,n}$  is the component of the free stream velocity that is normal to the camber at some point  $s$  on the camber. The other term,  $\omega'(s)$ , represents the contribution of the vortex sheet to the normal component of the velocity to the camber line. We find the term  $V_{\infty,n}$  where we take the components of the free stream velocity normal to the camber using the angle of attack as well as the angle of the camber. In this we use small angle approximations to consider  $\sin(\theta) \approx \theta$  and  $\tan^{-1}\theta \approx \theta$

$$V_{\infty,n} = V_\infty \left( \alpha - \frac{dz}{dx} \right) \quad (3.2)$$

We add the definition for  $\omega$  as

$$\omega(x) = -\frac{1}{2\pi} \int_0^c \frac{\gamma(\xi) d\xi}{(x - \xi)}. \quad (3.3)$$

Where  $\gamma(\theta)$  is the vortex strength. Finally, we put this in the equation 3.1 and perform a change of base and we end up getting -

$$\frac{1}{2\pi} \int_0^\pi \frac{\gamma(\theta) \sin \theta d\theta}{\cos \theta - \cos \theta_0} = V_\infty \left( \alpha - \frac{dz}{dx} \right). \quad (3.4)$$

Where the change of basis is as follows-

$$x = \frac{c}{2} (1 - \cos \theta_0) \text{ and } \xi = \frac{c}{2} (1 - \cos \theta) \quad (3.5)$$

Due to the presence of regions where the above equation is undefined, it is not directly solvable. So to solve this, we approximate this using the Glauert's method of solution [11].

$$\gamma(\theta) = \frac{V}{\pi} \{ A_0 \cot \frac{1}{2}\theta + A_1 \sin \theta + A_2 \sin 2\theta + A_3 \sin 3\theta + \dots \}, \quad (3.6)$$

This equation can be simplified to -

$$\gamma(\theta) = 2V_\infty \left( A_0 \frac{1 + \cos \theta}{\sin \theta} + \sum_{n=1}^{\infty} A_n \sin n\theta \right) \quad (3.7)$$

Next, we apply equation (3.7) back to the equation 3.4 and arrive at -

$$\alpha - \frac{dz}{dx} = A_0 - \sum_{m=1}^{\infty} A_m \cos m\theta \quad (3.8)$$

In this we must find the values of  $A_0$  and  $A_n$ . To do this, we first integrate both sides of the equation from 0 to  $\pi$ . This gives us just the  $A_0$  term which is as follows -

$$A_0 = \alpha - \frac{1}{\pi} \int_0^\pi \frac{dz}{dx} d\theta_0 \quad (3.9)$$

For the other terms, we multiply both sides by  $\cos(m\theta)$  and then integrate the solution from 0 to  $\pi$ . This removes the constant term and provides the desired values.

$$A_n = \frac{2}{\pi} \int_0^\pi \frac{dz}{dx} \cos n\theta_0 d\theta_0. \quad (3.10)$$

Now that we have completely defined  $\gamma(\theta)$ , we can find the circulation  $\Gamma$  over the airfoil, hence the generated lift  $L'$ .

$$\Gamma = \int_0^c \gamma(\xi) d\xi = \frac{c}{2} \int_0^\pi \gamma(\theta) \sin \theta d\theta. \quad (3.11)$$

$$L' = \rho_\infty V_\infty \Gamma = \rho_\infty V_\infty^2 c \left( \pi A_0 + \frac{\pi}{2} A_1 \right). \quad (3.12)$$

We use this equation of total lift to calculate the coefficient of lift as-

$$c_l = \frac{L'}{\frac{1}{2} \rho_\infty V_\infty^2 c(1)} = \pi(2A_0 + A_1). \quad (3.13)$$

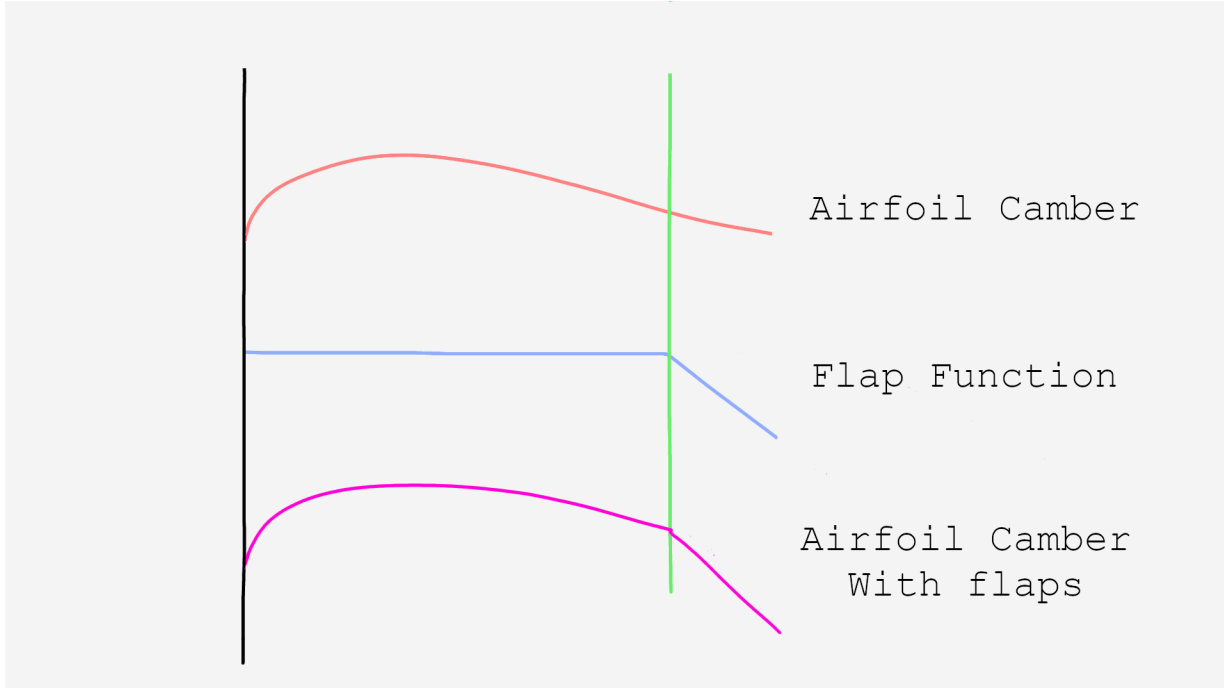
## 3.3 Wing With Flaps

### 3.3.1 Overview

The mathematical techniques used in the previous section are sufficient to include the effects caused by deployment of the flaps. The only modifications required for using the same algorithm will be replacing the shape of the camber with a new shape that replaces the trailing section of the camber with the flap geometry.

### 3.3.2 Mathematical Model

To obtain this new geometry, we need to deflect a small rear part of the airfoil downward. This is done by superimposing a deflection to the existing camber. The deflection is a mathematical function that is defined for all the points on the chord, which is zero for all values up to a certain value on the x axis (where the flap starts) and then the deflection can be considered to be a linear function with a constant slope. The slope here would be equivalent to the flap angle.



## 3.4 Blown Wing With Flaps

### 3.4.1 Overview

In his thesis titled "An Assessment of Electric STOL Aircraft", Courtin<sup>[12]</sup> gives us a good idea of the lift that is produced by an airfoil with a blown flap. However, the result provided in his thesis is limited to a flat airfoil with flaps that provide deflection to the exhaust jet. Since we need to compute the coefficient of lift for a cambered airfoil, we decided to ignore certain assumptions that Courtin<sup>[12]</sup> made. So, we build upon our existing model to estimate the  $C_L$  obtained in the case of wings with blown flaps.

### 3.4.2 Mathematical Model

Firstly we'll go through the method used by Courtin<sup>[12]</sup> for calculating the  $C_L$  for a flat airfoil. They have assumed an infinite wing with a thin and flat airfoil, and with a jet which is evenly spread over the airfoil such that there is a constant flow of the jet over the entire wingspan. The jet is also approximated as a vortex sheet similar to the airfoil.

We begin by considering that the jet has an inherent curvature  $\kappa = d\theta/ds$ . We relate this to the velocity change within the jet  $\Delta u$  and average jet velocity  $u_a$  as-

$$\Delta u = u_1 - u_2 = u_a \kappa h \quad (3.14)$$

Since the pressure is continuous across the jet boundaries, we consider the pressure difference in the external flow is the same as the pressure difference across the jet. Further, we use the Bernoulli's equation applied to both the inner flow as well as the jet. This gives with the following equation-

$$\frac{1}{2} \rho (V_1^2 - V_2^2) = \frac{1}{2} \rho_J (u_1^2 - u_2^2) \quad (3.15)$$

We then express this equation in the form of velocity jumps and average velocity as-

$$\rho V_a \Delta V = \rho_J u_a \Delta u = \rho_J u_a^2 \kappa h \quad (3.16)$$

We proceed to write the equation of the wake vortex strength by relating it to the velocity jump as-

$$\gamma_w = \Delta V - V_a \kappa h \quad (3.17)$$

We approximate the average velocity of the jet to be the same as the velocity of the jet at an infinite distance. We continue by defining the jet momentum per unit span as-

$$J' = \int_{-h/2}^{h/2} \rho u^2 dn \approx \rho_J V_J^2 h \quad (3.18)$$

We can write the expression of the vortex strength as-

$$\frac{\gamma_w}{V_\infty} = \frac{J' - \rho V_\infty^2 h}{\rho V_\infty^2} = \frac{\Delta J'}{\rho_\infty V_\infty^2} \quad (3.19)$$

We define a dimensionless coefficient  $\Delta c_J$ , which we will be calling our momentum-excess coefficient.

$$\Delta c_J \equiv \frac{\Delta J'}{\rho_\infty V_\infty^2 c} \quad (3.20)$$

We use this to approximate the vortex strength as-

$$\frac{\gamma_w}{V_\infty} \approx \frac{\Delta c_J}{2} c \frac{d\theta}{dx} \quad (3.21)$$

Finally, we use can formulate the equation of the streamline as-

$$\theta(x) \equiv \alpha + \frac{w(x)}{V_\infty} = \alpha + \frac{1}{2\pi} \int_0^c \frac{\gamma(\xi)}{V_\infty} \frac{d\xi}{\xi - x} + \frac{\Delta c_J}{2} \frac{1}{2\pi} \int_c^\infty \frac{d\theta}{d\xi} \frac{d\xi}{\xi - x} \quad (3.22)$$

Assuming a flat and thin airfoil, Spence [13] solved these equations, giving

$$c_\ell = \frac{\partial c_\ell}{\partial \alpha} \alpha + \frac{\partial c_\ell}{\partial \delta_F} \delta_F \quad (3.23)$$

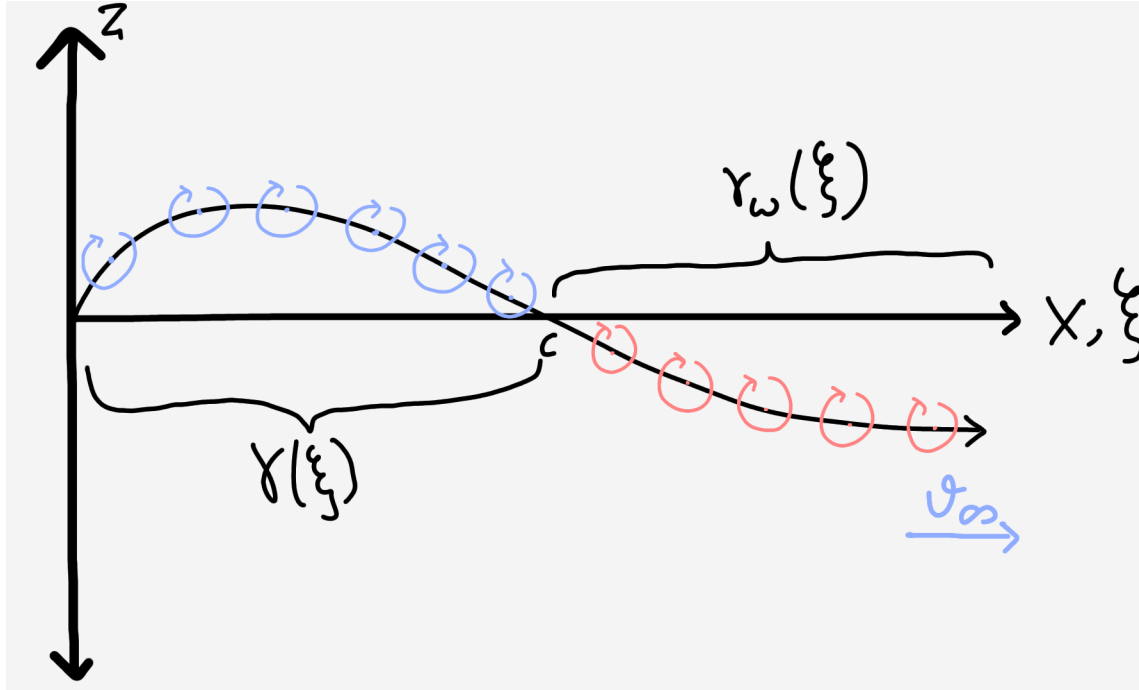
where

$$\frac{\partial c_\ell}{\partial \alpha} = 2\pi(1 + 0.151\sqrt{c_J} + 0.219c_J) \quad (3.24)$$

$$\frac{\partial c_\ell}{\partial \delta_F} = 2\sqrt{\pi c_J}(1 + 0.151\sqrt{c_J} + 0.139c_J)^{\frac{1}{2}} \quad (3.25)$$

Now to remove some of these approximations, we have used a different novel approach which is similar to the approach that we used to solve the basic thin airfoil.

We start by finding the value of the vortex strength. We cannot use exactly the same method as before 3.6 as this used the fact that the Kutta condition would have to be satisfied. However in the case of the blown flap, the Kutta condition is not satisfied entirely. For this, we divide the vorticity into two regions. One will be the region of the wing ( $x < c$ ), and the other region will be the region after the wing. We consider that the vorticity begins at the trailing edge of the wing and moves downwards eventually combining with the free stream velocity.



Thus, we expand our gamma as-

$$V_\infty \alpha(\theta) = \frac{1}{2\pi} \int_0^\pi \frac{\gamma(\phi)}{x(\theta) - x(\phi)} d\phi \gamma + \frac{1}{2\pi} \int_c^\infty \frac{\gamma_w(x')}{x(\theta) - x'} dx' \quad (3.26)$$

In this equation, the  $\gamma(\phi)$  term is such that the Kutta condition will be satisfied. Now going back to the equation 3.22, we notice that we can apply the Kutta condition to the  $\gamma(x')$  term. To do this, first we rearrange the equation as-

$$\frac{1}{2\pi} \int_0^c \frac{\gamma(x')}{V_\infty} \frac{dx'}{x' - x} = \theta(x) - \alpha - \frac{c \Delta c_J}{2} \frac{1}{2\pi} \int_c^\infty \frac{d\theta}{dx'} \frac{dx'}{x' - x} \quad (3.27)$$

Now we apply the Fourier series simplification 3.6 to the  $\gamma(\theta)$  term. We also substitute the value of  $\theta(x)$  as the camber line slope since this would be the path of the streamline over the airfoil. This simplifies the equation to-

$$A_0 - \sum_{m=1}^{\infty} A_m \cos m\theta = -\frac{dz}{dx} + \alpha + \frac{c \Delta c_J}{2} \frac{1}{2\pi} \int_c^\infty \frac{d\theta}{dx'} \frac{dx'}{\xi - x} \quad (3.28)$$

We use similar methods to what we used in our thin airfoil method to get the values of the constants. We start by integrating both sides from 0 to  $\pi$ . This removes all the cos terms meaning that we end up with the equation for the constant  $A_0$ . Making all these changes, we end up with the following equation-

$$A_0 = \alpha - \frac{1}{\pi} \int_0^\pi \left( \frac{dz}{dx} \right) d\theta + \frac{c \Delta c_J}{4} \frac{1}{\pi^2} \int_c^\pi \int_0^\infty \frac{d\theta}{dx'} \frac{dx'}{x' - x} d\theta \quad (3.29)$$

We use the equation 3.5 to change the basis and make the calculations easier.

$$A_0 = \alpha - \frac{1}{\pi} \int_0^\pi \left( \frac{dz}{dx} \right) d\theta + \frac{\Delta c_J}{2} \frac{1}{\pi^2} \int_c^\pi \int_0^\infty \frac{d\theta}{d\theta'} \frac{d\theta'}{\cos(\theta) - \cos(\theta')} d\theta' d\theta \quad (3.30)$$

Similarly, we multiply both sides with  $\cos(n\theta)$  and we integrate both sides from 0 to  $\pi$ . This removes the common term from the equation ( $A_0$ ) and we end up with the following-

$$A_n = -\frac{\Delta c_J}{2} \frac{c}{\pi^2} \int_0^\pi \int_0^\infty \frac{d\theta}{dx'} \frac{dx'}{x' - x} d\Theta + \frac{1}{\pi} \int_0^\pi \left( \frac{dz}{dx} \right) \cos(n\theta) d\theta \quad (3.31)$$

We also change the variable to make things easier

$$A_n = -\frac{\Delta c_J}{\pi^2} \int_0^\pi \int_0^\infty \frac{d\theta}{d\theta'} \frac{d\theta'}{\cos(\theta) - \cos(\theta')} d\Theta + \frac{1}{\pi} \int_0^\pi \left( \frac{dz}{dx} \right) \cos(n\theta) d\theta \quad (3.32)$$

Now, one of important things in this is defining the function of the jet streamline and how this merges with the free stream velocity. For this part, we refer to the solution provided by **S. H. Smith and M. G. Mungal**

$$\frac{y}{rd} = A \left( \frac{x}{rd} \right)^m \quad (3.33)$$

**S. H. Smith and M. G. Mungal** has stated the constants to be-  
 $A = 2.05$ ,  $m = 0.28$  for  $r$  within the range 5 to 35

We also need to find out the value of the effective velocity ratio ( $r$ ) which is given as-

$$r = \left( \frac{\rho_j U_j^2}{\rho_{cf} U_{cf}^2} \right)^{1/2}. \quad (3.34)$$

We use this equation to model the jet. For this, first need the find the point where the relative slope of the jet with respect to the free stream velocity is the same as the total effective angle of the end of camber.  $(\alpha + \frac{dz}{dx})$  This can be expressed mathematically as -

$$-\tan \left( \tan^{-1} \left( \frac{dz}{dx} \right) - \alpha \right) = Am(rd)^{1-m}(x)^{m-1} \quad (3.35)$$

After this, we must also use the 2D rotational matrix by an angle of  $-\alpha$  to align the end of the jet with the free stream velocity.

Now to find the coefficient of lift, we use similar methods to what we used before. We first start by defining the circulation which is the same as in equation 3.11. After this, we find the Lift and the coefficient of list which is the same as in equations 3.12 and 3.11. Thus we end up with our final equation as-

$$c_l = \frac{L'}{\frac{1}{2} \rho_\infty V_\infty^2 c(1)} = \pi(2A_0 + A_1). \quad (3.36)$$

Hence, this equation allows us to compute the coefficient of lift for cambered airfoils as well as those airfoils with flaps since we use the same method to deflect the camber of the airfoil to simulate the flap which we had used in the Section 2.3.2.

## 3.5 Finite Blown Wing with Flaps

### 3.5.1 Numerical Model

To extend our model to the third dimension, we use a method similar to the Prandtl Lifting Line model [14]. For this, we consider horseshoe vortices whose one edge is along the quarter chord of the wing and the other two edges extend to  $\infty$  which are perpendicular to the other vortex. We apply the no penetration condition which looks something like-

$$\frac{\partial \Phi_{\text{wing}}}{\partial z} + \frac{\partial \Phi_{\text{wake}}}{\partial z} + Q_\infty \alpha = 0 \quad (3.37)$$

Where,

$$w_b = \frac{\partial \phi_{\text{wing}}}{\partial z} = \frac{-\Delta \Gamma(y_0)}{4\pi[c(y)/2]} \quad (3.38)$$

and

$$w_i = \frac{\partial \phi_{\text{wake}}}{\partial z} = \frac{1}{4\pi} \int_{-b/2}^{b/2} \frac{[-d\Gamma(y_0)/dy]dy_0}{y - y_0} \quad (3.39)$$

Putting all of these into equation 3.37, we get the following result,

$$-\frac{\Gamma(y)}{\pi c(y)V_\infty} - \frac{1}{4\pi V_\infty} \int_{-b/2}^{b/2} \frac{[-d\Gamma(y_0)/dy]dy_0}{y - y_0} + \alpha = 0 \quad (3.40)$$

We experimented with the slope of the 2D blown airfoil ( $\alpha$  vs  $C_L$ ) and found that the slope could be approximated to a linear function in our region of interest ( $-10^\circ < \alpha < 10^\circ$ ). This allows us to express our  $C_l$  as a function of a slope which is as follows-

$$C_l = \frac{\rho V_\infty \Gamma(y)}{(1/2)\rho V_\infty^2 c(y)} = m_0(y) \alpha_e(y) \quad (3.41)$$

We express the effective angle with the camber as-

$$\alpha_e = \alpha - \alpha_i - \alpha_{L0} \quad (3.42)$$

In this,  $\alpha_{L0}$  is the angle at which zero lift is generated. We replace the *alpha* term in the equation as-

$$\frac{-2\Gamma(y)}{m_0(y)c(y)V_\infty} - \frac{1}{4\pi V_\infty} \int_{-b/2}^{b/2} \frac{[-d\Gamma(y_0)/dy]dy_0}{y - y_0} + \alpha(y) - \alpha_{L0}(y) = 0 \quad (3.43)$$

From this, we need to find the value of  $\Gamma$ . We do this using the Fourier series solution and also perform a change of base as-

$$\Gamma(\theta) = 2bV_\infty \sum_{n=1}^{\infty} A_n \sin(n\theta) \quad (3.44)$$

and,

$$y = -\frac{b}{2} \cos(\theta) \quad (3.45)$$

Using this equation, we get-

$$\alpha(\theta) - \alpha_{L0}(\theta) - \frac{4b}{m_0(\theta)c(\theta)} \sum_{n=1}^{\infty} A_n \sin(n\theta) - \frac{1}{\pi} \int_0^{\pi} \frac{\sum_{n=1}^{\infty} n A_n \cos n\theta_0}{\cos \theta_0 - \cos \theta} = 0 \quad (3.46)$$

$$\sum_{n=1}^{\infty} A_n \sin(n\theta) \left[ \frac{n}{\sin(\theta)} + \frac{4b}{m_0 c} \right] = \alpha(\theta) - \alpha_{L0}(\theta) \quad (3.47)$$

We simplify this equation using the Glaubert's integral [15], and using the obtained equations, we find the  $C_l$ . Therefore, the section lift and drag coefficients can be readily obtained:

$$C_l = \frac{\rho Q_\infty \Gamma(\theta)}{(1/2)\rho Q_\infty^2 c(\theta)} = \frac{4b}{c(\theta)} \sum_{n=1}^{\infty} A_n \sin n\theta$$

$$C_{d_i} = C_l \alpha_i = \frac{4b}{c(\theta)} \sum_{n=1}^{\infty} A_n \sin n\theta \left( \sum_{k=1}^{\infty} k A_k \frac{\sin k\theta}{\sin \theta} \right)$$

The wing aerodynamic coefficients are obtained by the spanwise integration of these section coefficients:

$$C_L = \int_{-b/2}^{b/2} \frac{C_l(y) c(y) dy}{S} = \frac{4b}{S} \int_0^{\pi} \sum_{n=1}^{\infty} A_n \sin n\theta \frac{b}{2} \sin \theta d\theta$$

$$C_{D_i} = \int_{-b/2}^{b/2} \frac{C_{d_i}(y) c(y) dy}{S} = \frac{2b^2}{S} \int_0^{\pi} \sum_{n=1}^{\infty} \sum_{k=1}^{\infty} k A_k A_n \sin k\theta \sin n\theta d\theta$$

The main task for us is to determine the coefficients  $A_1, A_2, \dots, A_n$ . This is determined by varying  $\theta$  in equation (4.47) from 0 to  $\pi$ . This can be done by taking  $n$  values of  $\theta$  between 0 and  $\pi$  and solve the system of linear equations using linear algebra. Thus we get all the coefficients. Only for  $n=k$  we get a non-zero value, rest all will be zero. Therefore:

$$C_L = \frac{\pi b^2 A_1}{S} = \pi AR A_1$$

$$C_{D_i} = \frac{\pi b^2}{S} \sum_{n=1}^{\infty} n A_n^2 = \pi AR \sum_{n=1}^{\infty} n A_n^2$$

Here due to symmetry we can observe that  $A_2, A_4, \dots, A_{2n}$  are zero. Hence we only consider  $A_1, A_3, \dots, A_{2n+1}$

# Chapter 4

## Computational Fluid Dynamics

### 4.0.1 Validation of Propulsion using Computational Fluid Dynamics

To validate the propulsion component of the STOL, we performed a Computational Fluids Dynamics (CFD) simulation in ANSYS 2025 R2 (Student Version) using a custom generated propeller. The objective was to achieve thrust within the given thrust to weight envelope with maximum possible efficiency at both take-off and cruise conditions.

#### 4.0.1.1 Geometry Construction and Meshing

The custom propeller is generated using a discrete radial function of airfoil chord length and twist. The diameter of the propeller is 130mm with the hub diameter being roughly 5mm. For our propeller, the chord and pitch distribution (w.r.t. the radius) are:

$$c(r) = -4984.325r^4 + 1582.915r^3 - 291.735r^2 + 14.513r + 0.0196 \quad (4.1)$$

$$\theta(r) = -19654967.194r^4 + 2358240.470r^3 - 87934.197r^2 + 420.644r + 67.390550 \quad (4.2)$$

For this particular propeller, our airfoil also varies with cross section (as is clearly visible), and the data for the airfoil geometry is kept in **Additional Files > propulsion > Propeller**.

For the sliding mesh method, an enclosure with radial cushioning of 10mm and axial cushioning of 5mm on both sides was given, this was allotted fluid domain and a further bigger box enclosure with cushioning of 150mm radially and 300mm and 400mm cushioning along the axial direction was given. The smaller enclosure is the rotating domain and the bigger one being the live domain.

Finally, we performed "Boolean Subtract" operations to generate a rotating domain without the propeller body and a boolean operation between the live and rotating domain.

Finally, overall mesh body sizing of 40mm element sizing and face sizing of 15mm element sizing was used to generate optimum mesh, keeping in mind the computational resources available.

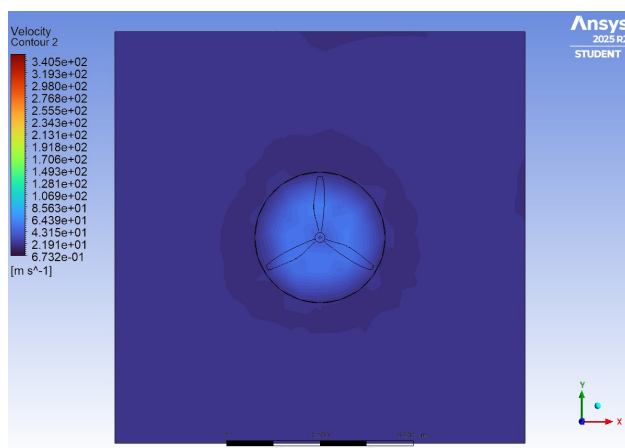
#### 4.0.1.2 Setup

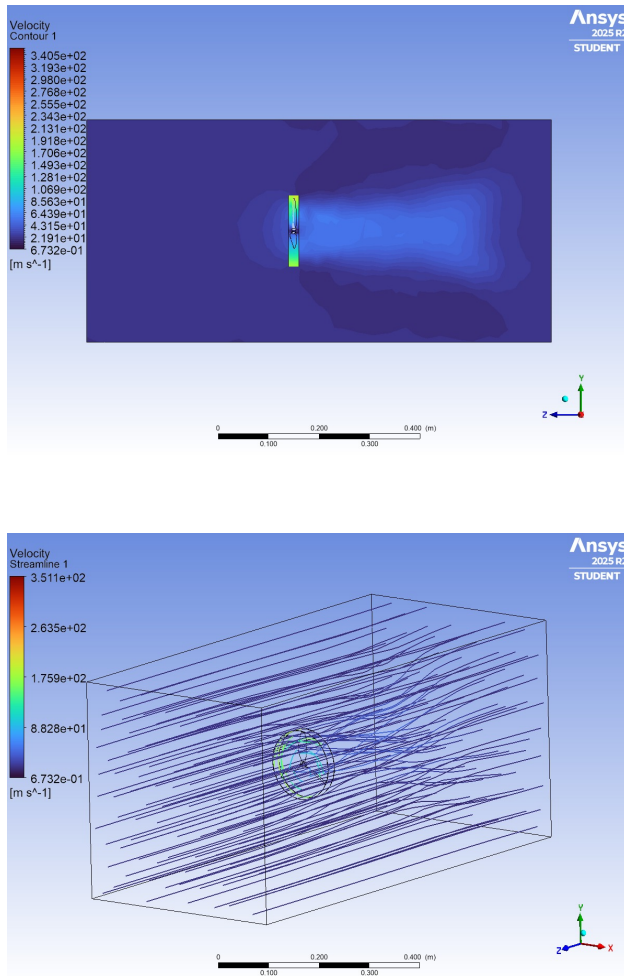
We used standard air properties in the setup. The solver was set up based on standard practices for this type of aerodynamic simulation.

- **Solver Type:** Pressure-Based, Transient.
- **Turbulence Model:** We selected the  $k - \epsilon$  model set to "Realisable" and the Scalable-wall function option enabled.
- **Solution Methods:** We used the SIMPLE scheme with Second Order Up - wind discretization for momentum and turbulence, Gradient set at Least Squares Cell Based. This provides a stable and highly accurate solution.
- **Boundary Conditions:**
  - Inlet: Set as a Velocity Inlet with magnitude  $20m/s$ . This was applied to the C-shaped arc and the flat top/bottom boundaries.
  - Outlet: Set as pressure outlet with  $0Pa$  gauge pressure.
  - Walls: Set the specified shear as 0 in all directions.
- **Initialization:** We used Hybrid Initialization to get a good starting guess for the solver. We set the convergence criteria for all residuals to  $1 \times 10^{-4}$  to ensure a fully converged solution.
- **Cell Zone Conditions:**
  - rotating domain: The Mesh Motion option was enabled with rotation axis co-ordinates set to global origin and rotation axis direction set to "Z-axis". The rotational Speed was set to 27,000rpm.

#### 4.0.1.3 Results and Discussion

After running the simulation, we obtained the Thrust = 18.24N and exported the pressure and velocity contour plots.





We obtained the thrust values with the Time Step value set to 0.00015sec, Number Time steps set to 100 and Iterations per time step set to 15.

#### 4.0.2 Validation of Wing Design using Computational Fluid Dynamics

To validate the accuracy of the mathematical model from the previous section, we performed a Computational Fluid Dynamics (CFD) simulation in Ansys 2025 R2 using the same NACA 4412 airfoil (9 cm chord and 100 cm span). The objective was to determine the  $C_L$  and  $C_D$  values at a 10-degree Angle of Attack, which serves as a reliable benchmark for our results.

##### 4.0.2.1 Geometry Construction and Meshing

We began our simulation by importing the .step file of the NACA 4412 airfoil with a chord length (L) of 9cm and a span (S) of 100cm. After importing this file into ANSYS DesignModeler, we created an enclosure with a downstream length of 4 m, which is more than 20 times the chord length and is sufficient for accurate simulation. The enclosure

dimensions were set to 1.5 m in the y-direction and 0.5 m in the z-direction, considering our limit of 1 million cells in ANSYS.

Finally, we performed a ‘Boolean’ operation to subtract the airfoil shape from the fluid domain. This leaves an “airfoil-shaped hole” which acts as the solid wall. We then changed the property of the enclosure to be a fluid domain.

To make sure the meshing was done correctly, we applied face sizing on all faces of the airfoil and made the size approximately 10 times smaller than the general mesh size.

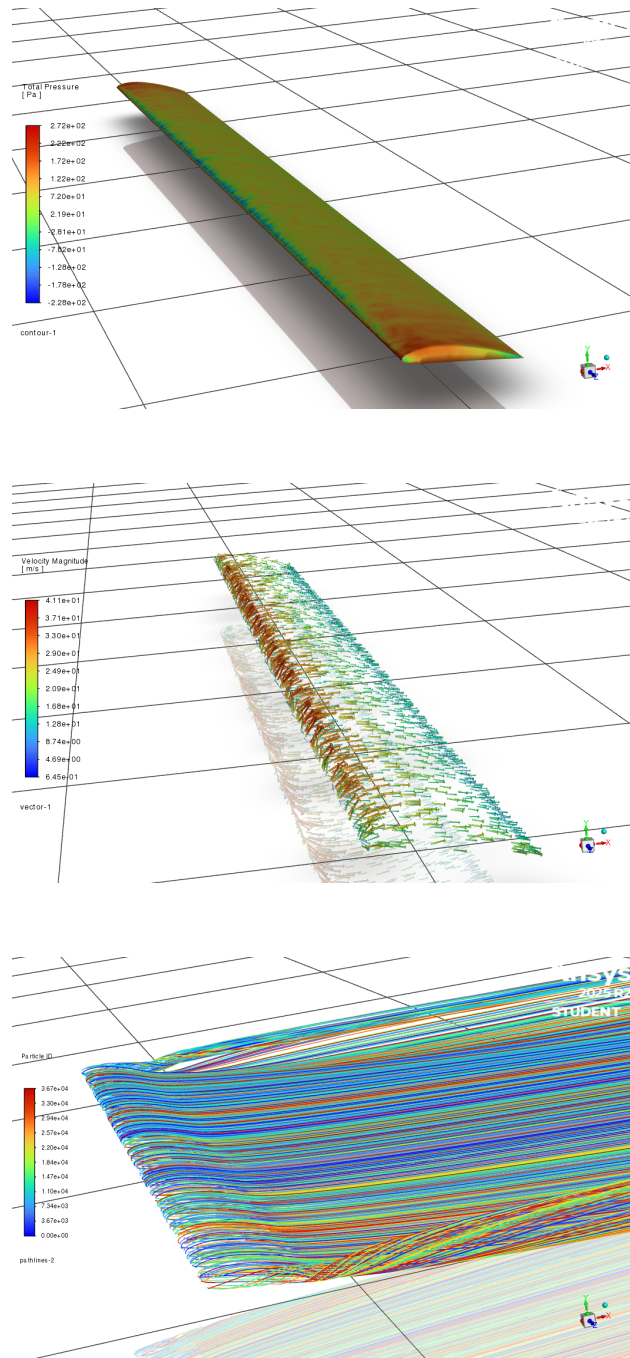
#### 4.0.2.2 Setup

We used standard air properties in the setup. The solver was set up based on standard practices for this type of aerodynamic simulation.

- **Solver Type:** Pressure-Based, Steady-State.
- **Turbulence Model:** We selected the SST (Shear Stress Transport)  $k - \omega$  model. This is the best choice because it accurately predicts flow near the wall and also handles the freestream flow well.
- **Solution Methods:** We used a Coupled pressure-velocity scheme with Second Order Up - wind discretization for momentum and turbulence, Gradient set at Green-Gauss Node Based. This provides a stable and highly accurate solution.
- **Boundary Conditions:**
  - Inlet: Set as a Velocity Inlet with magnitude  $20\text{m/s}$ . This was applied to the C-shaped arc and the flat top/bottom boundaries.
  - Outlet: Set as pressure outlet with  $0\text{Pa}$  gauge pressure.
  - Airfoil: Set as a no-slip Wall.
  - Walls: Set the specified shear as 0 in all directions.
- **Initialization:** We used Hybrid Initialization to get a good starting guess for the solver. We set the convergence criteria for all residuals to  $1 \times 10^{-4}$  to ensure a fully converged solution.

#### 4.0.2.3 Results and Discussion

After running the simulation, we obtained the  $C_L = 1.1649$  and  $C_D = 0.0781$  value for  $\alpha = 10\text{ deg}$  and exported the pressure and velocity contour plots.



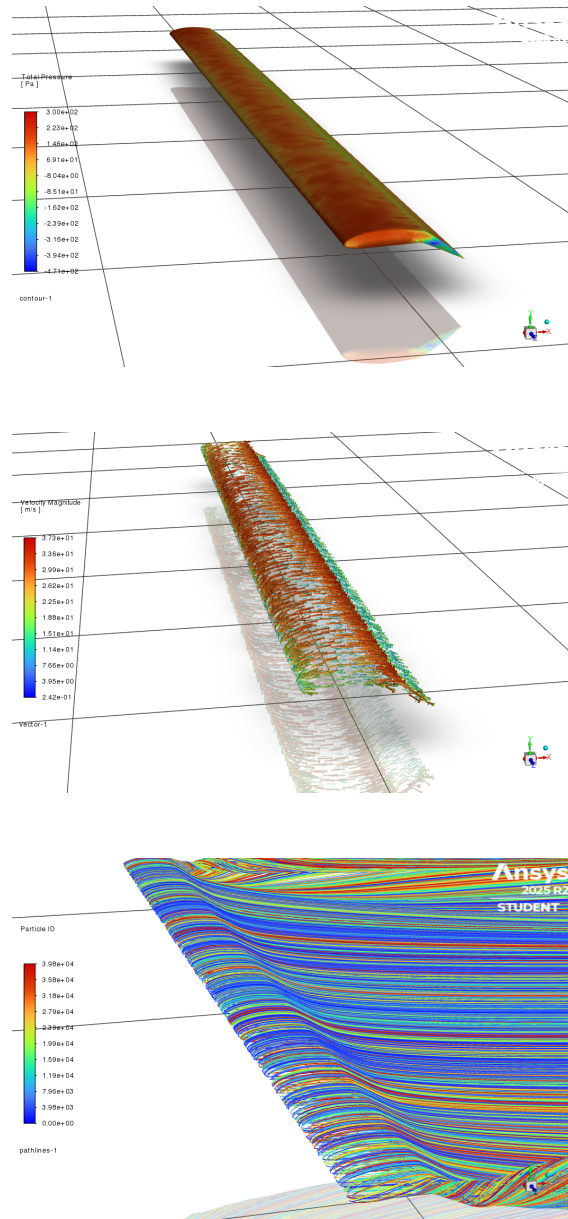
We obtained lift and drag convergence at approximately the 40th iteration, and we continued the simulation up to 250 iterations using hybrid initialization.

### 4.0.3 Adding Flaps

Similar Techniques as the previous section would be needed for doing the analysis of a wing with flaps. The only modification will be the wing and flap geometry(pitch angle = 30 degree and 30 percent chord length), as CFD tools can accurately estimate the fluid flow characteristics in these kinds of situations.

#### 4.0.3.1 Results and Discussion

After running the simulation, we obtained the  $C_L = 1.7615$  and  $C_D = 0.1420$  value and exported the pressure and velocity contour plots.



We obtained lift and drag convergence at approximately the 40th iteration, and we continued the simulation up to 200 iterations using hybrid initialization.

#### 4.0.4 Validation of Blowing Characteristics using Computational Fluid Dynamics

To validate the blown flap wing of the STOL using the propulsion component discussed earlier, we performed a Computational Fluids Dynamics (CFD) simulation in ANSYS 2025

R2 (Student Version) using a custom generated propeller. The objective was to achieve the required lift at cruise and take-off conditions.

#### 4.0.4.1 Geometry Construction and Meshing

The geometry included 6 propellers with a NACA 4412 wing with flaps deployed at an angle of 30 degrees. The 6 propellers were aligned parallel to the wing geometry and were equidistant along the span. The geometry of the propellers stayed consistent, and the geometry of the wing was as follows: Span= 1250mm and Chord length = 100mm.

For Moving Reference Frame method, individual enclosures for all the propellers were generated with an average cushioning of 1mm. The overall box cushioning of 100mmx100mm and axial cushioning of 250mm and 350mm in positive and negative directions

Finally, we performed "Boolean Subtract" operations to generate a rotating domain without the propeller body and a boolean operation between the live and rotating domain.

Finally, overall mesh body sizing of 160mm element sizing and face sizing of 20mm element sizing was used to generate optimum mesh, keeping in mind the computational resources available.

For Meshing we performed face meshing at the airfoil and the propellers for more accurate results.

#### 4.0.4.2 Setup

We used standard air properties in the setup. The solver was set up based on standard practices for this type of aerodynamic simulation.

- **Solver Type:** Pressure-Based, Steady-State.
- **Turbulence Model:** We selected the  $k - \epsilon$  model set to "Realisable" and the Scalable-wall function option enabled.
- **Solution Methods:** We used the SIMPLE scheme with Second Order Up - wind discretization for momentum and turbulence, Gradient set at Least Squares Cell Based. This provides a stable and highly accurate solution.
- **Boundary Conditions:**
  - Inlet: Set as a Velocity Inlet with magnitude  $20m/s$ . This was applied to the C-shaped arc and the flat top/bottom boundaries.
  - Outlet: Set as pressure outlet with  $0Pa$  gauge pressure.
  - Walls: Set the specified shear as 0 in all directions.
- **Initialization:** We used Hybrid Initialization to get a good starting guess for the solver. We set the convergence criteria for all residuals to  $1 \times 10^{-4}$  to ensure a fully converged solution.
- **Cell Zone Conditions:**

- rotating domain: For all rotating domains, Frame Motion option was enabled with rotation axis coordinates set to global origin and rotation axis direction set to "Z-axis". The rotational Speed was set to 15,000rpm.

#### 4.0.4.3 Results and Discussion

After running the simulation, we obtained the  $C_L = 6.528$  and exported the streamline plots. We obtained lift and drag convergence at approximately the 100th iteration, and we continued the simulation up to 175 iterations using hybrid initialization.

# Chapter 5

## Final Results

### 5.0.1 Introduction

In this section, we will be using our mathematical model to find out our final parameters for the wing. We will be using our BEMT, and DEP mathematical models to do this.

### 5.0.2 Propeller Geometry

We have used a high thrust and low axial speed propeller as required for a STOL and below are its geometry specifications:

Table 5.1: Propeller Blade Geometry at Radial Stations

r (mm)	Pitch (deg)	Chord Length (mm)
76.71	67.37	89.19
165.1	64.00	152.40
276.2	56.70	200.92
393.7	50.00	228.60
476.2	46.94	232.17
723.9	40.00	177.80
925.0	20.00	76.20

### 5.0.3 Airfoil Geometry

From iterative analysis of using various airfoils for calculating  $C_L$  and consequent  $L/D$  ratio we found out that the airfoil "NACA-4412" to be the best suited for achieving the desired configuration as mentioned in the problem statement. All the used airfoils can be found in "Additional Files/wing/Airfoils"

### 5.0.4 Take Off Configuration

For this, we run our DEP mathematical model to find out the maximum  $C_L$  achievable while also ensuring that our  $\frac{C_L}{C_D}$  ratio is maintained to be over 5. For this we will be running our

DEP\_takeoff.py code (path - /LATAerospace/Additional Files/wing). We apply some initial parameters as follows-

- Free Stream velocity :  $20m/s$
- Percentage Flaps : 30%
- Flap Angel :  $20^0$
- Propeller Diameter : 0.13 meters
- Chord Length : 0.1 meters
- Wingspan : 1.25 meters
- Angle of Attack =  $7^0$

Note that in this, we are using the outputs that we get from the BEMT analysis for the sea level analysis at an airspeed of  $20m/s$ .

With these inputs, we are able to get the output as follows-

Coefficient of Lift: 7.05575402,

Induced drag : 1.38225639,

Lift to drag ratio : 5.10451901

From these results, we can see that we have achieved the following design targets-

Coefficient of Lift > 6.5 (Achieved : 7.05575402)

Lift to drag ratio > 5 (Achieved : 5.10451901)

Lift > 15kg (Achieved : 22.046875)

### 5.0.5 Cruise Configuration

To calculate the Coefficient of Lift, Lift-to-Drag Ratio and to limit the calculated values under the given specifications we run over "Additional Files/wing/DEP\_cruise.p". For cruise we assume the flaps to be retracted and with this we ensure  $\frac{C_L}{C_D} > 20$ .

- Free Stream velocity :  $80m/s$
- Percentage Flaps : 0%
- Flap Angel :  $0^0$
- Propeller Diameter : 0.13 meters
- Chord Length : 0.1 meters
- Wingspan : 1.25 meters
- Angle of Attack =  $0^0$

We have obtained the following:

Coefficient of Lift:  $C_L = 0.61206$

Induced Drag:  $C_{D_i} = 0.01055842$

Lift to Drag Ratio:  $\frac{C_L}{C_D} = 57.97$

We must also ensure that the lift obtained for the given  $C_L$  must be greater than the assumed weight of the aircraft.

In essence,

$$\frac{1}{2}\rho V_\infty^2 C_L = \text{Lift} > 15g$$

thus,  $222.22 = \text{Lift} > 15g$ , hence our aircraft cruises.

From these results, we can see that we have achieved the following

Lift to Drag Ratio  $> 20$

## Combined Simulation Results

The table below consolidates all calculated aerodynamic and propulsion system performance data across two primary flight conditions: Takeoff/Sea Level and Cruise.

Table 5.2: Detailed Summary of All Calculated Performance Metrics

Condition	Parameter	Value	Unit
<i>Aerodynamic Coefficients (from DEP_takeoff.py)</i>			
	Lift Coefficient $C_L$	7.055	—
	Induced Drag Coefficient $C_{D_i}$	1.389	—
	Lift to Drag Ratio $L/D$	5.104	—
<b>Takeoff / Sea Level</b>	<i>Propulsion Metrics (at V=20 m/s)</i>		
	Velocity $V$	20.00	m/s
	RPM	15316.24	—
	Thrust	90.69	N
	Efficiency	23.40	%
	Pitch Collective	14.53	deg
<b>Cruise</b>	<i>Aerodynamic Coefficients (from DEP_cruise.py)</i>		
	Lift Coefficient $C_L$	0.612	—
	Induced Drag Coefficient $C_{D_i}$	0.0105	—
	Lift to Drag Ratio $L/D$	57.97	—
	<i>Propulsion Metrics (at V=80 m/s)</i>		
	Velocity $V$	80.00	m/s
	RPM	18367.682	—
	Thrust	75.00	N
	Efficiency	54.01	%
	Pitch Collective	19.80	deg

# Chapter 6

## Structural Analysis

### Formulas Used

#### Lift (total) for the entire wing

$$L = qSC_L$$

#### Dynamic pressure

$$q = \frac{1}{2}\rho V^2$$

#### Elliptical lift distribution

If a spanwise distribution is needed rather than a uniform pressure, an elliptical load approximation is used:

$$l(y) = l_0 \sqrt{1 - \left(\frac{2y}{b}\right)^2}$$

Peak per-unit-span load:

$$l_0 = \frac{4L}{\pi b}$$

Approximate local surface pressure (distributed over the chord  $c$ ):

$$p(y) \approx \frac{l(y)}{c}$$

### Takeoff Condition

Given:

$$C_L = 0.7, \quad V = 80 \text{ m/s}, \quad \rho = 0.909 \text{ kg/m}^3,$$
$$S = 1.25 \times 0.1 \text{ m}^2$$

Span and chord from area expression:

$$b = 1.25 \text{ m}, \quad c = 0.1 \text{ m}$$

## Aerodynamic results

Dynamic pressure:

$$q = \frac{1}{2}\rho V^2 = 0.5(0.909)(80^2)$$

Total lift:

$$L = qSC_L = 189.9N$$

Peak local pressure at the root (approx):

$$p_{\text{root}} \approx \frac{l_0}{c} = 1934 \text{ Pa}$$

## Cruise Condition

Given:

$$C_L = 6.2, \quad V = 20 \text{ m/s}, \quad \rho = 1.225 \text{ kg/m}^3,$$

$$S = 1.25 \times 0.1 \text{ m}^2$$

Assume full span:

$$b = 1.25 \text{ m}$$

## Lift Computation

Dynamic pressure:

$$q = \frac{1}{2}\rho V^2 = 0.5(1.225)(20^2)$$

Total lift:

$$L = qSC_L = 254N$$

## Elliptical Lift Distribution (for root bending moment)

Peak per-unit-span load:

$$l_0 = \frac{4L}{\pi b}$$

Taking:

$$c = 0.1 \text{ m}$$

Peak local pressure at root:

$$p_{\text{root}} = \frac{l_0}{c}$$

Maximum pressure condition used for structural simulation:  $p_{\text{root}} = 2558 \text{ Pa}$

So, we performed the structural simulation for the maximum pressure condition, that is 2558 Pa.

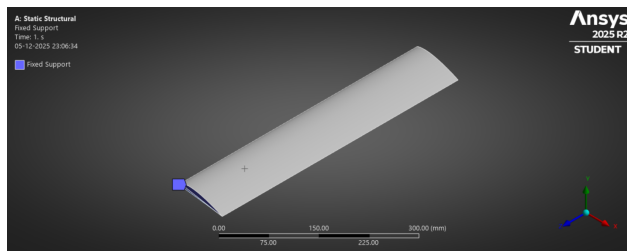


Figure 6.1: Support

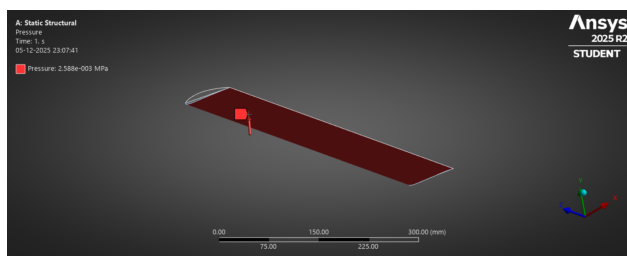


Figure 6.2: Applied Pressure

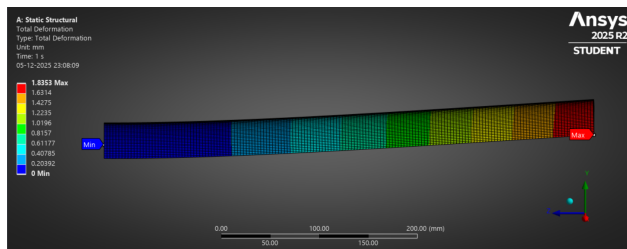


Figure 6.3: Deformation

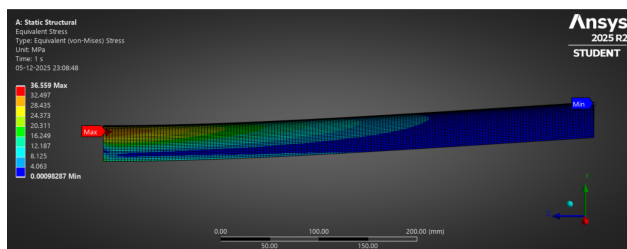


Figure 6.4: Equivalent Stresses

# **Chapter 7**

## **End Comments**

### **7.1 Additional Features**

#### **7.1.1 Inboard-Up Rotation Mechanism**

In this method<sup>[16]</sup> propellers are placed on the wingtips such that the swirl induced by the propeller is upwards on the inboard side and downwards on the outboard side. This basically means that the swirl that is generated by the propellers opposes the wing tip vortices. This swirl recovery helps in reducing the induced drag and also increases the wings apparent aspect ratio.

#### **7.1.2 Tilting Down of the Propeller**

We induce a downward tilt to the propeller, the lift increases and the drag decreases significantly<sup>[16]</sup>. This amplifies the upwash on the upgoing blade side while it reduces it on the downgoing blade side.

#### **7.1.3 Counter Rotating Blades or Wing twist**

Due to the swirl effect of the propeller, on part of the wing will be under the influence of an up-wash effect while the other will be under the influence of a downwash effect. This leads to one side experiencing a higher apparent angle of attack while the other experiences a lower apparent angle of attack. This means that at high angles of attack of the plane, one section under the influence of the jet of the propellers would stall while the other would be under-performing. This can be tackled by either introducing counter rotating blades, or introducing a twist in the wing such that the apparent angle of attack would be the same throughout. This allows us to operate the aircraft under more aggressive angles of attack without having to worry about stalling. [17]

# Bibliography

- [1] S. V. Karen Deere Jeffrey Viken and M. Carter, "Computational analysis of a wing designed for the x-57 distributed electric propulsion aircraft," *AIAA Aviation Forum*, 2017.
- [2] Electra. "Home | electra.aero." Accessed: 12 November 2025. [Online]. Available: <https://electra.aero>.
- [3] H. Winarto, "Bemt algorithm for the prediction of the performance of arbitrary propellers," 2004.
- [4] Wikipedia. "Regula falsi method of false position. "[Online]. Available: [https://en.wikipedia.org/wiki/Regula\\_falsi](https://en.wikipedia.org/wiki/Regula_falsi).
- [5] J. G. Leishman, *Principles Of Helicopter Aerodynamics*. Cambridge University Press, 2000.
- [6] G. W. S. THEODORE THEODORSEN and M. J. BREVOORT, "Characteristics of six propellers including the high-speed range," *NATIONAL ADVISORY COMMITTEE FOR AERONAUTICS*, 1937.
- [7] a. J. C. P. J. Morgado M. Â. R. Silvestre, "Validation of new formulations for propeller analysis," *JOURNAL OF PROPULSION AND POWER*, 2015.
- [8] W. H. Gray, "Wjnd-tunnel tests of two ramiltcn standard propellers embodynm clark y and naca 16-series blade sectloos," 1941.
- [9] N. A. P. Nikolas S. Zawodny Noah H. Schiller, "Aerodynamic and acoustic characterization of a ducted propeller in a small hover anechoic chamberaerodynamic and acoustic characterization of a ducted propeller in a small hover anechoic chamber," NASA, Tech. Rep., 2025.
- [10] *Prediction of Lift*. MIT. [Online]. Available: [https://web.mit.edu/16.unified/www/SPRING/fluids/Lecture\\_Notes/f18.pdf](https://web.mit.edu/16.unified/www/SPRING/fluids/Lecture_Notes/f18.pdf).
- [11] L. M. Thomson, *Theoretical Aerodynamics*. Dover Publications, 1958.
- [12] C. B. Courtin and R. J. Hansman, "An assessment of electric stol aircraft," M.S. thesis, Massachusetts Institute of Technology, 2019. [Online]. Available: <https://hdl.handle.net/1721.1/122042>.
- [13] D. A. Spence, "The lift coefficient of a thin, jet-flapped wing," [Online]. Available: <https://royalsocietypublishing.org/doi/10.1098/rspa.1956.0203>.
- [14] J. Katz and A. Plotkin, *Low-Speed Aerodynamics*. Cambridge University Press, 2001.

- [15] J. L. Yves-Marie Scolan, "On some integrals of glauert's type," *Applied Mathematics Letters*, 2004.
- [16] L. Veldhuis, "Review of propeller-wing aerodynamic interference," *ICAS*, 2004.
- [17] A. M. Stoll and J. Bevirt, "Drag reduction through distributed electric propulsion]," *American Institute of Aeronautics and Astronautics*, 2014.